ELSEVIER

Journal of Alloys and Compounds 434–435 (2007) 13–17

Journal of ALLOYS AND COMPOUNDS

www.elsevier.com/locate/jallcom

Deformation behavior of a $Ti_{66}Cu_8Ni_{4.8}Sn_{7.2}Nb_{14}$ nanostructured composite containing ductile dendrites

J. Eckert [a,b,*], J. Das [a,b], K.B. Kim [a,c], F. Baier [a], W. Löser [b], M. Calin [d], Z.F. Zhang [e], A. Gebert [b]

[a] *Physical Metallurgy Division, Department of Materials and Geo Sciences, Darmstadt University of Technology, Petersenstraße 23, D-64287 Darmstadt, Germany*

[b] *Leibniz-Institute for Solid State and Materials Research Dresden, D-01171 Dresden, Germany*

[c] *Department of Advanced Materials Engineering, Sejong University, 98 Gunja-dong, Gwangjin-gu, Seoul 143-747, Korea*

[d] *University "Politehnica" of Bucharest, Materials Science and Engineering Faculty, Spl. Independentei 313, Bucharest R-060032, Romania*

[e] *Shenyang National Laboratory for Materials Science, Institute of Metal Research, Chinese Academy of Sciences, 72 Wenhua Road, Shenyang 110016, China*

Available online 2 October 2006

Abstract

The deformation behavior of multicomponent $Ti_{66}Cu_8Ni_{4.8}Sn_{7.2}Nb_{14}$ composite containing primary dendrites embedded in a nanoeutectic matrix was studied under uniaxial compression. The evolution of slip and shear bands has been investigated at various stages of deformation. This type of advanced composite not only displays a high compressive plasticity of 31.8%, but also exhibits high fracture strength of ≈2.02 GPa (true fracture strength 1.38 GPa). Pronounced work hardening was observed after yielding. The surface deformation morphology reveals that the work hardening behavior of the composite is related to the plastic deformation of the dendritic phase through slip bands and the interaction of shear bands in the nanostructured matrix with the hardened dendrites. The nucleation of shear band occurs at a certain amount (8%) of plastic deformation at the dendrite–nanoeutectic matrix interface. The final stage of compression proceeds through passing of the shear bands through the work-hardened dendrites into the nanoeutectic matrix, whereby the propagation of the shear bands in the matrix is retarded by the nanoscale phases.

Keywords: Nanostructured composite; Microstructure; Mechanical properties; Deformation mechanism; Shear bands

1. Introduction

In recent years, many attempts have been made to improve the ductility of nanostructured and glassy alloys [1–9]. As one example, in situ formed dendrite phase reinforced nanoeutectic composites show a dramatic increase in plastic strain under compression, providing an effective way to synthesize nanostructured alloys with improved ductility [1,2]. In particular, substantially improved mechanical properties have been obtained recently in in situ formed Ti-based nanostructure–dendrite composites with plastic strains larger than 15% and fracture stresses higher than 2 GPa [10,11]. The enhanced ductility of such composites is attributed to the dendrites dispersed in the matrix, acting as obstacles hindering the rapid propagation of shear bands, thus controlling the instability otherwise responsible for early failure [12,13]. Recently, a systematic investigation on Ti-base nanoeutectic composites [14,15] using transmission electron microscopy revealed a stepped morphology of the interface between the dendrites and the nanoeutctic matrix that is generated by passing of the shear bands. The improved mechanical properties combined with the potential for engineering applications of these composites [1,10,11] have prompted us to search for the details of the deformation mechanisms, which impart both improved strength and ductility. This is crucial, since the deformation and fracture mechanisms of these composites have not been well understood, yet.

In this paper, a $Ti_{66}Cu_8Ni_{4.8}Sn_{7.2}Nb_{14}$ nanostructured composite is selected as an example from a series of high strength-ductile Ti–Cu–Ni–Sn–Nb alloys [11]. The microscopic deformation behavior and the evolution of slip and shear bands in this nanostructured matrix/ductile dendritic phase composite have been investigated after different extent of deformation. The enhanced ductility of the Ti-based composite will be discussed

* Corresponding author at: IFW Dresden, Institut für Festkörperanalytik und Strukturforschung (IFS) Postfach 27 01 16, D-01171 Dresden, Germany. Tel.: +49 351 4659 602; Fax: +49 351 4659 452.

E-mail address: j.eckert@ifw-dresden.de (J. Eckert).

0925-8388/$ – see front matter © 2006 Elsevier B.V. All rights reserved.
doi:10.1016/j.jallcom.2006.08.198

in terms of the deformation mechanisms of the ductile dendritic phase and its role in resisting the propagation of shear bands.

2. Experimental

The $Ti_{66}Cu_8Ni_{4.8}Sn_{7.2}Nb_{14}$ alloy was solidified through cold crucible casting (10 mmØ, 180 mm long) after mixing of the pure elements and characterized by X-ray diffraction (XRD) using a Philips D500 diffractometer with Cu Kα radiation. The microstructure and the phases present in the alloy were examined by a Zeiss 962 scanning electron microscope (SEM), a high resolution SEM (Philips XL 30) and transmission electron microscopy (TEM) (Philips CM 20). Bar shape compression specimens were prepared by machining of the as-cast specimen to 2 mm × 2 mm cross-section and 4 mm height. The surfaces were polished and etched to observe the as-cast microstructure, also allowing for the following observation of the surface deformation morphology. Compression tests were performed using a Schenck hydraulic testing machine under quasistatic loading (strain rate of 8×10^{-4} s^{-1}) at room temperature on two different type of specimens: (A) samples deformed up to a plastic strain of $\varepsilon_p = 8.1\%$ and then unloaded, and (B) samples deformed up to a strain of $\varepsilon_p = 24.5\%$ and then unloaded (cf. the stress–strain curves in Fig. 2). One specimen has been compressed until fracture. After compression, the surface deformation morphology of the specimens was examined using a Zeiss 962 scanning electron microscope (SEM). Thin slices were prepared from the deformed specimens ($\varepsilon_p = 24.5\%$) and were investigated using transmission electron microscopy (TEM, Philips CM 20).

3. Results and discussion

The as-cast alloy shows a composite microstructure consisting of coarse dendrites embedded in a dark matrix. The overall microstructure of the alloy is presented in Fig. 1. A high resolution SEM image (inset in Fig. 1) of the matrix shows the presence of an eutectic microstructure consisting of 150 nm wide and 500–800 nm long Ti_2Cu rods in an α-Ti solid solution, which was also confirmed by TEM studies [14,15]. The volume fraction of the dendrites was estimated to be 80–90 vol.%. The compression test results of the as-cast sample are consistent with an earlier report [11]. A typical engineering stress–strain curve up to failure is presented in Fig. 2 (thick line). The mechanical properties are as follows: yield strength $\sigma_{0.2} = 940 \pm 25$ MPa, plastic strain $\varepsilon_p = 28 \pm 2\%$, and maximum

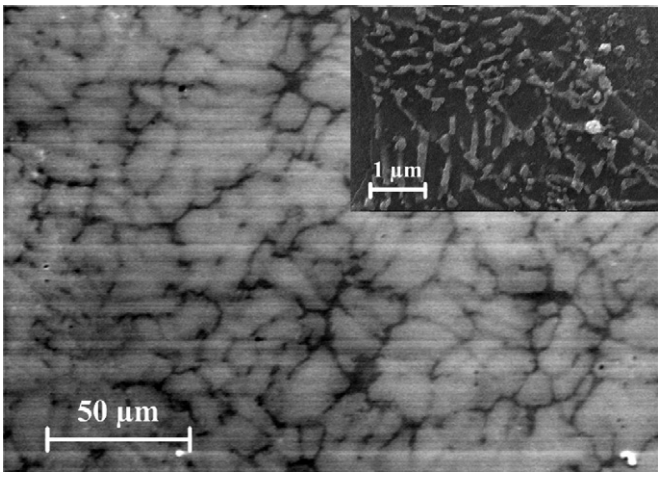

Fig. 1. SEM secondary electron image of the as-cast microstructure of the Ti-base nanostructure–dendrite composite; inset: magnified image of the nanoeutecic matrix showing the presence of Ti_2Cu rods in a hcp α-Ti phase.

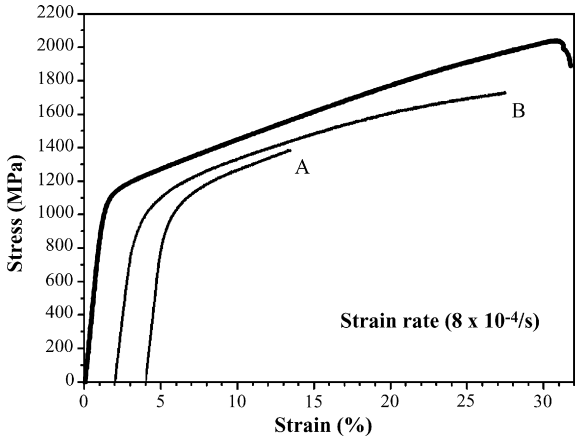

Fig. 2. Compressive stress–strain curve of up to: (A) 8.1%, and (B) 24.5% plastic strain and up to failure (thick curve).

strength $\sigma_{max} = 2000 \pm 25$ MPa (true fracture strength 1.38 GPa) with a noticeable work hardening behavior. The specimen surface shows a large number of shear bands and viscous shear flow traces, as observed earlier [11].

In an attempt to investigate the deformation mechanism of this ductile composite, as-cast specimens have been compressed to different amount of plastic strain and unloaded. The corresponding compressive stress–strain curves are presented in Fig. 2 and marked as (A) for a sample deformed to $\varepsilon_p = 8.1\%$ and (B) for a sample deformed to $\varepsilon_p = 24.5\%$. It is worth to note that the XRD patterns (not shown here) reveal no significant difference between the as-cast and the deformed samples subjected to different amount of plastic strain, and the fractured sample, indicating that there was no phase transformation during the deformation.

Fig. 3(a) shows the overall features of specimen A. At this stage ($\varepsilon_p = 8.1\%$) no barreling of the specimen was observed. The specimen surfaces are quite parallel. Very fine bands can be found on the specimen surface. The density of these bands is very high and their growth is restricted within the dendrites. There is no preferred orientation of these bands with the stress axis. Since work-hardening of the composite is clear from the stress–strain curve (A), these bands must be 'slip bands' that form due to dislocation movement in the dendrites. Typical features of such fine profuse slip bands are presented in Fig. 3(b) and marked by small white arrows. The thick black arrows indicate the direction of the applied stress. In addition, in most regions the dendrites show 'wrinkle'-like features along with a high density of slip bands at the center of the specimen. This indicates that the initiation of the localized deformation is related to both the high-strength nanostructured matrix and the ductile dendrites. At this stage it is anticipated that some of the grains in the nanoeutectic matrix may contribute to the strain via dislocation movement. Interestingly, in a region close to the "wrinkled" dendrites, a few shear bands are observed to pass through the dendrites, as indicated by a dotted white arrow in Fig. 3(b). However, the majority of the area on the specimen surface does not display this feature. These bands are relatively sharper than the slip bands and have different contrast. The overall features suggest that there might be a preferred orientation with the applied stress

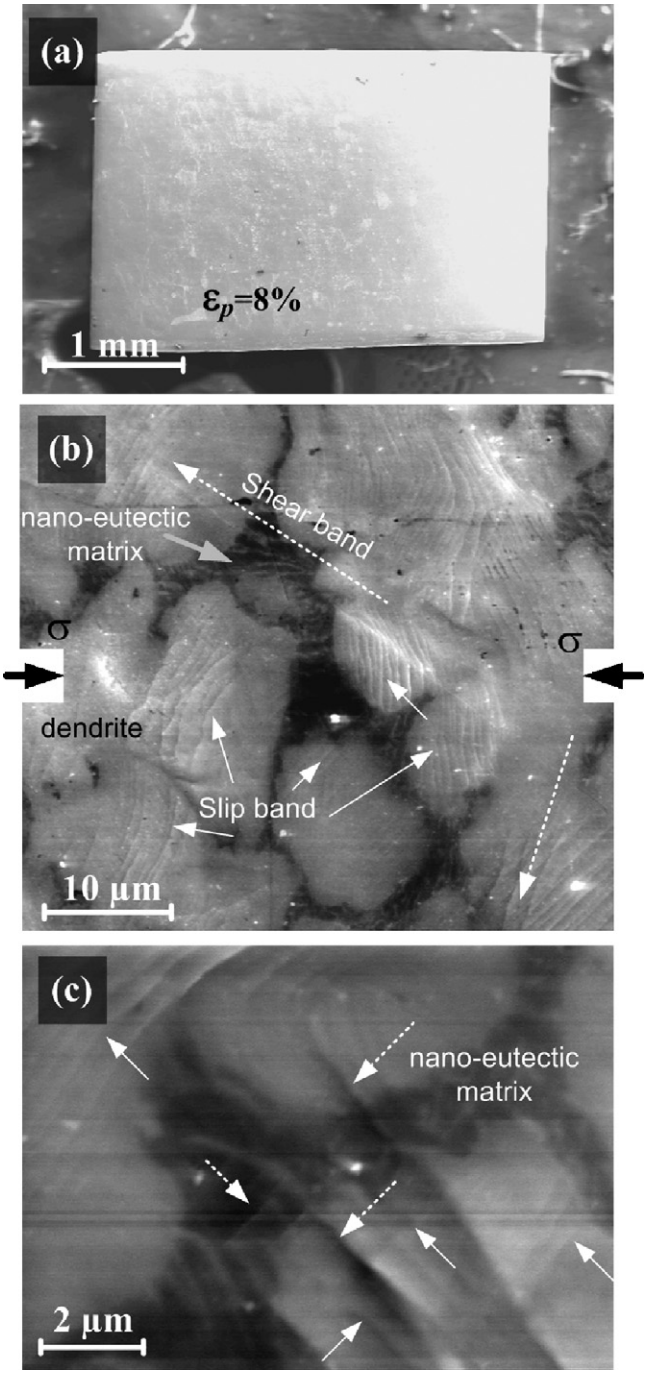

Fig. 3. Microstructural features of the specimen deformed to ($\varepsilon_p = 8.1\%$): (a) overview, (b) formation of slip bands (small arrows) in the dendrites, and (c) nucleation of shear bands at the dendrite–nanoeutectic matrix interface (dotted arrows).

axis. Since the strain distribution is not completely homogenous in the material, these observations validate that the initial deformation originates from dislocation movement and the formation of slip bands inside the dendrites and proceeds through shear banding. A magnified image of a set of parallel shear bands passing through the interface between the nanoeutectic matrix and the dendrite is shown in Fig. 3(c). The initiation of shear bands moving perpendicular to the former direction is also visible in the dark nanostructured matrix (Fig. 3(c), dotted arrows).

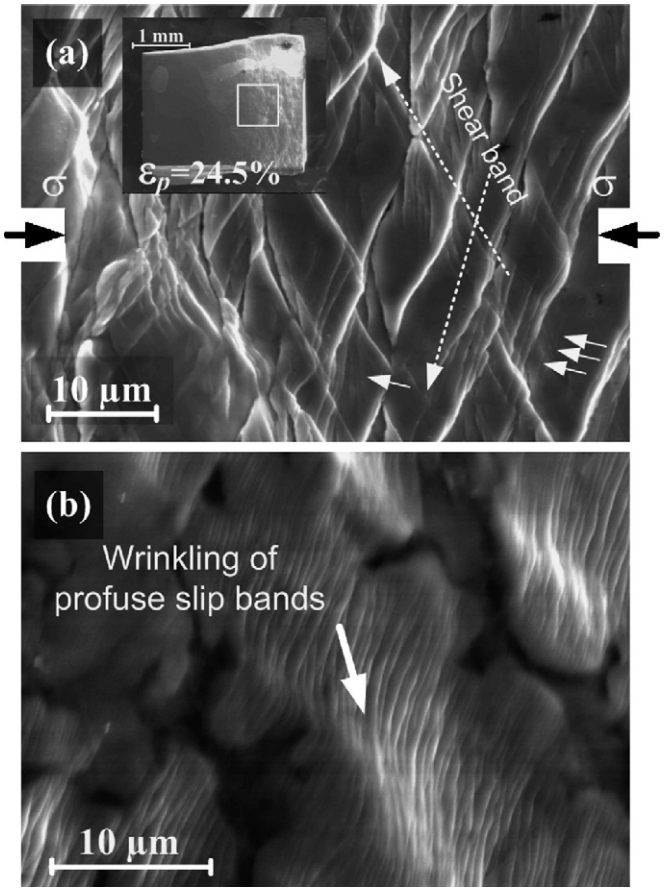

Fig. 4. Microstructural features of the specimen deformed to ($\varepsilon_p = 24.5\%$): (a) formation of highly dense shear bands (dotted arrows) and their impingement along with slip bands (small arrows); inset: overview and (b) wrinkling of the dendrites with profuse slip bands.

Thus, the plastic strain for nucleating the visible (microscopic scale) shear bands in this composite is close to 8%. A similar result (plastic strain = 5–13%) was also observed earlier for a $Ti_{62}Cu_{14}Ni_{12}Sn_4Nb_8$ composite [13]. It is very clear from this image that the contrast of the 'shear band' (dotted arrows) is more pronounced than for the 'slip bands' (small arrows). This may be due to the fact that the amount of shear-offset and strain relief for the shear bands is higher than for the slip bands.

The surface of the 24.5% deformed specimen (Fig. 2, curve B) shows remarkably different features in comparison to the specimen subjected to only 8% plastic strain. The strongly deformed sample is buckled and barreled, as shown in the inset of Fig. 4(a). In addition, the formation of highly dense shear bands on the specimen surface was observed throughout the sample. An enlarged view of the region marked by a square in the inset of Fig. 4(a) is shown in Fig. 4(a). The direction of the applied stress is indicated by thick black arrows. A large number of impingement and intersection events of the shear bands under primary and secondary direction are observed on the specimen surface, as depicted in Fig. 4(a). The shear band spacing is on the order of 5–10 μm. The intersection of the shear bands moving to different direction creates steps on each other, which finally appear similar like the surface of a 'pineapple'. This indicates that the density of the shear bands increases rapidly with further strain beyond 8%.

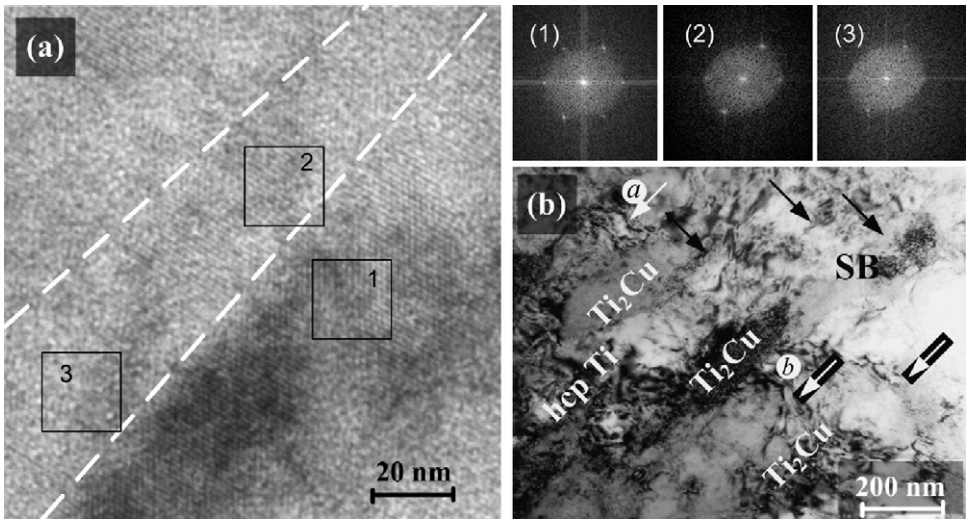

Fig. 5. (a) HR-TEM image of the apex of a shear band and the Fourier transformed patterns [1, 2, and 3] from the corresponding different regions of the image marked as 1, 2 and 3. (b) Passing of the shear bands through the nanoeutectic matrix.

A region away from the center of the specimen shows extensive wrinkling of the dendrites with profuse slip bands (Fig. 4(b)). The shape of some dendrite arms changes from an elliptical to a flat shape at the direction normal to the loading axis. From the stress–strain curve a distinct work hardening can be observed. However, the microstructure cannot be clearly resolved in the severely deformed regions. Inside the inter-shear band regions a high density of slip bands can be observed. Thus, the work-hardening of the composite at this stage is stems from: (i) the formation of new slip bands and their wrinkling, (ii) the impingement of the shear bands with neighboring slip bands in the dendrite, and (iii) locking of the primary and secondary shear bands.

Further analysis [14–16] based on TEM investigations of the 24.5% deformed specimen revealed a stepped morphology at the interface between the dendrites and the nanoeutectic matrix. The slip transfer from the nanostructured matrix to the dendrites is believed to initiate such a stepped morphology due to passing of shear bands without generating cracks. A triangle-shape contrast is often observed around the intersection regions between the shear bands aligned to two directions inside the dendrites. A high-resolution image from the apex of a shear band inside a dendrite is presented in Fig. 5(a). The Fourier transformed pattern from region 1 (Fig. 5(a)) from a dendrite of the deformed $Ti_{66.1}Cu_8Ni_{4.8}Sn_{7.2}Nb_{13.9}$ alloy clearly reveals the diffraction of a bcc lattice along the [1 1 1] direction. The intensity of the diffraction spots continuously decreases inside the shear band at region 2 and completely disappears at region 3. This indicates that inside the shear band typical amorphous-like and distorted/disordered lattice fringes can coexist due to extensive local lattice distortion in highly strained areas within the dendrites in regions 2 and 3, as shown in Fig. 5(a). On the other hand, passing of the shear bands (primary and secondary) through the nanoeutectic matrix has also been clearly observed. Fig. 5(b) shows the existence of shear bands, which are aligned perpendicular to each other in the nanoeutectic matrix, as marked by the white and black arrows. The passing of the shear bands into the matrix becomes easier when propagating under a direction almost parallel with the nanoscale Ti_2Cu rods (marked by the white arrows) in the hcp Ti matrix. On the other hand, the nanoscale Ti_2Cu rods hinder the propagation of the shear bands when they are aligned under a perpendicular direction, as evidenced in Fig. 5(b) (marked by black arrows). Fig. 5(b) shows that the shear bands (white arrows) are significantly deflected at the interfaces of the Ti_2Cu phase (at point a). After a few layers of the eutectic rods (Ti_2Cu phase) the shear band regenerates (at point b) and propagates through the nanoeutectic matrix, detouring the following Ti_2Cu phase. This indicates that the nucleation and restricted propagation of shear bands is also controlled by the nanometer-scale eutectic matrix.

4. Conclusion

The $Ti_{66}Cu_8Ni_{4.8}Sn_{7.2}Nb_{14}$ composite exhibits work hardening after yielding. The maximum strength and plastic strain are ~2.02 GPa (true fracture strength 1.38 GPa) and ~32%, respectively. With further compression after yielding, strong work hardening of the composite results in the formation of fine slip bands in the dendrites and subsequent activation of shear bands at the dendrite–matrix interface at ~8% plastic strain. A high density of shear band develops and mainly propagates in the matrix or at the matrix/dendrite interface at higher strain level (24.5%). This might result from the strengthening effect of the dendritic phase and pronounced wrinkling of profuse shear bands, which finally helps to nucleate new shear bands, and the restriction of their rapid propagation by the hardened dendrites. The accumulation of a high strain level in the shear bands causes local lattice distortion and even amorphization in the dendrites.

Acknowledgements

The authors thank G. He, M. Heilmaier, M. Kusy, G. Miehe, and R. Theissmann for technical assistance and simulating discussions, and U. Kunz for TEM sample preparation.

Funding by the EU within the framework of the Research Training Network on ductile bulk metallic glass composites (MRTN-CT-2003-504692) is gratefully acknowledged.

References

[1] G. He, J. Eckert, W. Löser, L. Schultz, Nat. Mater. 2 (2003) 33.
[2] J. Das, W. Löser, U. Kühn, J. Eckert, S.K. Roy, L. Schultz, Appl. Phys. Lett. 82 (2003) 4690.
[3] J. Das, M.B. Tang, K.B. Kim, R. Theissmann, F. Baier, W.H. Wang, J. Eckert, Phys. Rev. Lett. 94 (2005) 205501.
[4] J. Schroers, W.L. Johnson, Phys. Rev. Lett. 93 (2004) 255506.
[5] Z. Bian, H. Kato, C.L. Qin, W. Zhang, A. Inoue, Acta Mater. 53 (2005) 2037.
[6] C.C. Koch, J. Metast. Nanocryst. Mater. 18 (2003) 9.
[7] D.V. Louzguine, H. Kato, A. Inoue, Appl. Phys. Lett. 84 (2004) 1088.
[8] J.S. Park, H.K. Lim, J.H. Kim, J.M. Park, W.T. Kim, D.H. Kim, J. Mater. Sci. 40 (2005) 1937.
[9] Y.C. Kim, D.H. Kim, J.C. Lee, Mater. Trans. JIM 44 (2003) 2224.
[10] G. He, W. Löser, J. Eckert, Acta Mater. 51 (2003) 5223.
[11] G. He, J. Eckert, W. Löser, M. Hagiwara, Acta Mater. 52 (2004) 3035.
[12] E. Ma, Nat. Mater. 2 (2003) 7.
[13] H. Zhang, X.F. Pan, Z.F. Zhang, J. Das, K.B. Kim, C. Müller, F. Baier, M. Kusy, A. Gebert, G. He, J. Eckert, Z. Metallkd. 96 (2005) 675.
[14] K.B. Kim, J. Das, F. Baier, J. Eckert, Appl. Phys. Lett. 86 (2005) 171909.
[15] K.B. Kim, J. Das, F. Baier, J. Eckert, Appl. Phys. Lett. 86 (2005) 201909.
[16] J. Eckert, J. Das, K.B. Kim, Z.F. Zhang, G. He, F. Baier, C. Müller, Intermetallics, (accepted).